

CORROSION BEHAVIOR OF COMMERCIALY-PURE TITANIUM WITH DIFFERENT MICROSTRUCTURES

КОРРОЗИОННОЕ ПОВЕДЕНИЕ ТЕХНИЧЕСКИ ЧИСТОГО ТИТАНА С РАЗЛИЧНОЙ МИКРОСТРУКТУРОЙ

Lead. Res., Dr. Semenov V.I.^{1,2,+}, Prof., Dr. Huang S.-J.³, Prof. Tontchev N.⁴, Jun. Res. Valiev R.R.², Jun. Res. Belov P.A.², PhD Stud. Bogale D.³, PhD Stud. Wang A.³

¹SASI Institute for Strategic Studies, RB, Ufa, Russia

²Ufa State Aviation Technical University, Ufa, Russia

³National Taiwan University of Science and Technology, Taipei, Taiwan

⁴"Todor Kableshtov" Higher School of Transport, Sofia, Bulgaria

⁺corresponding author, e-mail: semenov-vi@rambler.ru

Abstract. This paper reports on the results of corrosion tests, using alternative methods, of Grade 4 CP Ti samples with coarse-grained (annealed) and ultrafine-grained structures after severe plastic deformation processing. The effect of microstructure on the corrosion of the material under study is demonstrated. It is revealed that the material with a UFG structure has a higher corrosion resistance, as compared to the samples with a CG structure.

KEY WORDS: CORROSION; COMMERCIALY PURE TITANIUM; COARSE-GRAINED AND ULTRAFINE-GRAINED STRUCTURE; SEVERE PLASTIC DEFORMATION.

1. Gravimetric corrosion test

Introduction

Owing to a great interest in the production of high-strength implants for medical applications from commercially pure (CP) titanium, one turns, more and more often, to the technologies based on severe plastic deformation. These technologies enable producing a high-strength state due to the the formation of an ultrafine-grained (UFG) structure that contributes to a significant enhancement of mechanical and functional properties [1, 2].

Promising is the use of high-strength long-length materials with a UFG structure [3], in particular, from CP Ti [4] which can be used for the production of medical implants that are, in particular, in frictional contact in saline medium.

Relatively recently, studies focused on a comparative evaluation of the corrosion resistance of materials with a coarse-grained and UFG structure were initiated [5]. For instance, it was demonstrated in [6] that in the investigated materials (low- and medium-carbon steels), having a UFG structure after severe plastic deformation (SPD) processing by equal-channel angular pressing (ECAP), an increase in corrosion resistance is observed. It may be assumed that a similar effect should be expected for CP Ti as well.

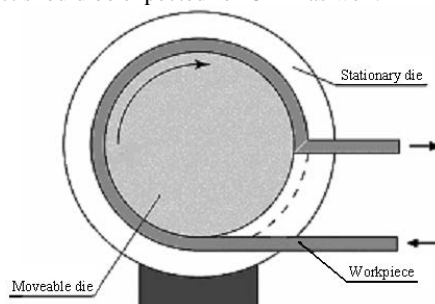


Fig. 1 Principle of the ECAP-Conform technique for the fabrication of long-length semi-products

After SPD processing, specimens with a length of 25 mm were cut out from the produced rods, for the deposition of ion-plasma coating and surface treatment by microarc oxidation. One specimen was left uncoated. In a similar manner, specimens were prepared from the annealed samples having a CG structure.

Corrosion tests were performed by immersion in 3.5% sodium chloride aqueous saline solution. Fig. 3 shows the diagram of the unit used to perform the corrosion tests.

The immersion tests were carried out in a waterproof thermostat during 28 hours at a temperature of $40 \pm 0.2^\circ\text{C}$.

There are known works on the fabrication of semi-products from CP Ti for medical applications, having a UFG structure, processed by SPD [7-9] followed by deposition of coatings from titanium nitride [7, 8] and diamond-like carbon with zirconium [9].

At the current stage of research, an express evaluation has been performed, of the corrosion properties of CP Ti, depending on the structural state and the presence of a coating on the surface of the investigated material in the coarse-grained (CG) and UFG states.

1.1. Material and research procedure

As the material for the study, CP Ti Grade 4 was used, with a CG structure in the annealed condition, and with a UFG structure in the SPD-processed condition. Fig. 1 shows the principle of the SPD technique employed to process the material.

The SPD processing of the material was conducted at a temperature of 400°C in 6 processing cycles, with rotation of the billet by 90° around its axis after each cycle. Fig. 2 shows the produced long-length samples from CP Ti Grade 4.



Fig. 2. CP Ti samples after SPD processing

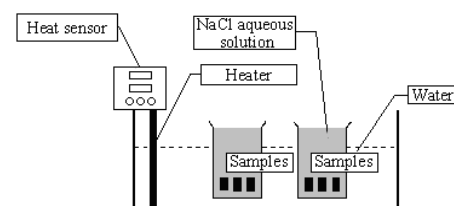


Fig. 3. Principle of the immersion tests

Metallographic studies were performed, using optical and transmission microscopes.

1.2. Research results

Given below are the results of the metallographic studies. Fig. 4 shows an example of microstructure transformation as a result of SPD processing.

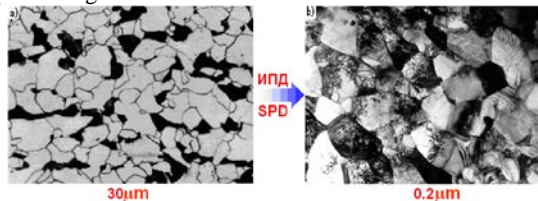


Fig. 4. Transformation of the material's microstructure as a result of SPD processing: a) coarse-grained structure of the material in the initial state; b) ultrafine-grained structure of the material after SPD processing

Table 1. Results of corrosion tests

Specimens	Coarse-grained structure (CG)			Ultrafine-grained structure (UFG)		
	Uncoated	Ion-plasma coating	Microarc oxidation	Uncoated	Ion-plasma coating	Microarc oxidation
Initial mass	9.003	8.960	8.436	9.185	9.133	8.787
28 hours	8.993	8.958	8.435	9.182	9.132	8.786
Mass loss, %	0.11104%	0.02232%	0.01185%	0.03266%	0.01095%	0.01138%

For the sake of visualization, the results of the corrosion tests are presented in the form of a bar chart in Fig. 5.

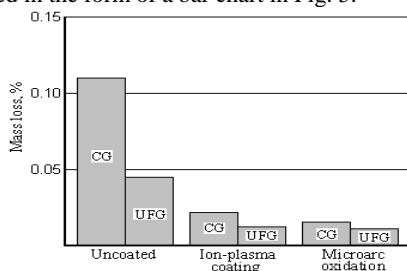


Fig. 5. The results of comparative corrosion tests: CG denotes the coarse-grained material after annealing; UFG denotes the ultrafine-grained material after SPD processing

As can be seen from the preliminary results of the corrosion tests (Fig. 6), the type of the applied coating (ion-plasma deposition and microarc oxidation) has practically no effect on the extent of corrosion damage. The differences between them fall within the statistical error. This may indicate a rather high protective capability of both coating types. At the same time, it is noted that the uncoated material after SPD processing in the UFG state has a considerably lesser degree of corrosion damage, as compared with the initial (annealed) state with a coarse-grained structure. The corrosion rate of the uncoated specimens from CP Ti Grade 4 in two structural states was evaluated. Fig. 6 shows the variation of mass loss depending on the time that the specimens were held in the 3.5% NaCl saline solution.

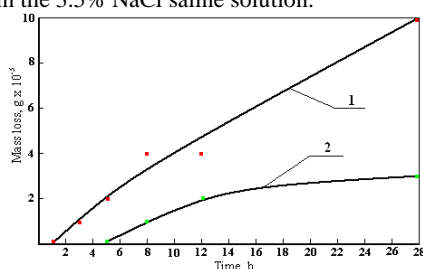


Fig. 6. Corrosion rate of CP Ti Grade 4: 1 denotes the CG structure after annealing; 2 denotes the UFG structure after SPD processing

As a result of metallographic studies, it has been established that in the initial state the microstructure of CP Ti represents an equiaxed structure with a mean grain size of 30 μm . The deformation processing by ECAP leads to an efficient grain structure refinement, with the mean grain size equal to 0.2 μm .

As was already noted above, before conducting the corrosion tests, an ion-plasma coating of TiC composition was deposited on the surface of some specimens, and some specimens were processed by microarc oxidation. As a result of the processing by microarc oxidation of specimens with different microstructures, an oxide film of TiO composition was formed on the surface of CP Ti. When studying the film formed through the use of either technology, it was established that its thickness was $3 \pm 0.3 \mu\text{m}$.

The results of corrosion tests are given in Table 1.

As can be seen from this graph the specimens with a CG structure (curve 1) exhibit a much higher corrosion rate, as compared to the specimens with a UFG structure (curve 2) in the accepted time interval. The variation of mass loss for the CG material in the selected time range has a practically linear character. In contrast, for the specimens with a UFG structure there is observed an area with a small slope of the curve, which indicates a decrease in the corrosion rate. In addition, it is noted that for the specimens with a CG structure, the start of the corrosion process is recorded after the first hour of testing, whereas for the specimens with a UFG structure, the first signs of the starting mass loss are observed only after five hours of testing.

Presumably on the material with UFG structure in connection with more advanced and extended total grain boundary these layers form a dense, almost impermeable barrier, due to which corrosion is strongly inhibited or completely stopped. Passivation is carried out chemically or electrochemically. In the latter case, conditions are created when metal ions under the influence of current pass into a solution containing ions, the ability to form very slightly soluble compounds. This assumption requires further study of the corrosion behavior of commercially pure titanium with different microstructure in an aqueous solution of sodium chloride using electrochemical methods with the formation of anodic and cathodic curves.

These observations require more detailed investigations to study the mechanism of corrosion damage of CP Ti with different microstructures.

2. Electrochemical corrosion tests

Introduction

The high corrosion resistance of CP Ti is conditioned by its self-passivation. In a weak-acid medium, the corrosion of non-passivated Ti is the result of two coupled reactions: the anodic reaction $\text{Ti} - 2\text{e} = \text{Ti}^{2+}$ and the cathode reaction $2\text{H}^+ + 2\text{e} = \text{H}_2$.

2.1. Experimental procedure

The polarization curves were recorded according to the three-electrode scheme, using a silver-chloride reference electrode and a platinum auxiliary electrode. The samples were polished with abrasive papers of decreasing grit size and a diamond paste, afterwards they were degreased with a White Spirit solution and

installed into a three-electrode cell with a 3.5% NaCl + 3% CH₃COOH solution until the equilibrium potential was reached. The potential sweep was conducted from the equilibrium potential to ± 400 mV with a rate of 1 mV per second.

2.2. Results and discussion

In Fig. 7 the anodic reaction is displayed by the initial region of the curve, demonstrating a transition from active dissolution to the onset of passivation at the potential E_p and full passivation at the potential E_{fp} ; for the UFG samples passivation occurs at larger potentials than for CG samples, but the current of passivation onset for the CG sample is slightly higher.

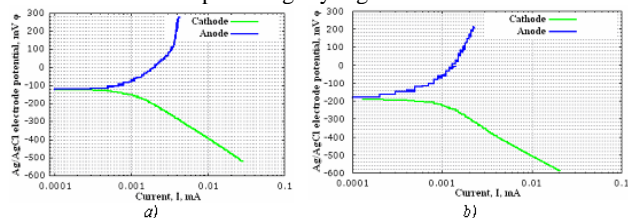


Fig. 7. Polarization curves for CP Ti: a) – with a CG structure; b) – with a UFG structure

The cathodic reaction of hydrogen evolution runs with a smaller overpotential. Consequently, the process of titanium's corrosion in a weak acid electrolyte takes place with anodic control.

The corrosion currents determined by the extrapolation of the Tafel regions of the anodic and cathodic curves amount to 0.97 μ A and 0.62 μ A, respectively, for the CG and UFG samples. Thus, the corrosion current of the CG sample in a weak acid electrolyte is 1.56 times higher than the corrosion current of the UFG sample (see table 2).

Table 2. Corrosion currents

Sample	Corrosion current, μ A
UFG	0.62
CG	0.97

The features of the corrosion behavior of CP Ti in the CG and UFG states may be associated with the self-passivation phenomenon. For instance, the perimeter of grain boundaries in the UFG sample is larger than the one in the CG sample, while the surface binding energy of atoms is lower. At the same time, on the surface there forms a continuous and thick oxide film due to a large amount of free enthalpy. As it can be seen in fig. 7, the equilibrium potentials of corrosion are more positive (-1.2 V) for the CG sample (Fig. 7, a) and less positive (-1.85 V) for the UFG sample (Fig. 7, b).

Proceeding from this, not taking into account the passivating properties of the oxide film on titanium, the CG sample is supposed to possess a lower corrosion activity than the UFG sample. However, as demonstrated by the analysis of polarization curves, the corrosion current of the CG sample is more than 1.5 times higher than the corrosion current of the UFG sample. In this connection, one may assume that the properties of the forming oxide film have a significant effect on the corrosion properties of CP Ti.

The differences in the formation of oxide passivating layer on Ti can be indirectly observed in the last third of the anodic branch of the polarization curves, displayed in fig. 7. As it can be seen in Fig. 7, a, the induced current continues to become further saturated, also after the overpotential of 0.2 V, and remains practically unchanged with increasing potential; this may indicate the maximum ionization current of Ti in this electrolyte solution. In Fig. 7, b the linear region is less expressed, but after it ends, the titanium, with increasing potential, continues to dissolve with growing induced current, its values being smaller than the ones for the CG sample; this may indicate larger diffusion limitations for the anodic process, created by the oxide film, in UFG Ti as compared to CG Ti.

In addition to the corrosion tests performed according to the two above-described procedures, clarifying tests in a salt spray chamber were conducted as an alternative method.

3. Corrosion tests in a salt spray chamber

3.1. Experimental procedure

The tests were performed in accordance with the ASTM G31 standard [10] in vapor atmosphere in a salt spray chamber, its schematic diagram being shown in Fig. 8. The size of the tested samples from CP Ti with CG and UFG structures was 9 x 25 x 9 mm. The concentration of the NaCl salt solution was 3.5%. The duration of the experiment was 10 days.

Corrosion resistance was evaluated on the basis of weight loss. The weight loss was recorded in accordance with the requirements of the ASTM G1 standard [11]. The samples were weighed on an analytical balance after withdrawal from a reservoir and careful washing in distilled water with a soft brush, followed by removal of water with filter paper.

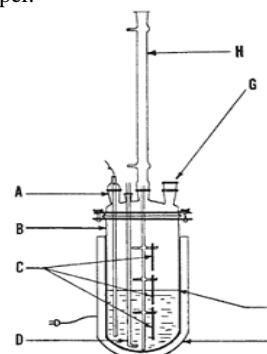


Fig. 8. Schematic diagram of the salt spray chamber. A – thermowell; B – reservoir with a solution; C – samples suspended on holders; D – air duct; E – reservoir heater; F – fluid surface; G – hole for the connection of the reservoir to an auxiliary device that may be required; H – reflux condenser.

The salt spray chamber is a reservoir that can be used as a universal and convenient apparatus for conducting simple corrosion tests. The configuration of the reservoir's upper portion is such that more complex devices can be added to it, depending on the specific test type.

3.2. Test results

The area of corrosion damage was estimated in accordance with the recommendations set forth in CNS8886 [12]. According to the quantitative evaluation, the larger is the score, the smaller is the corrosion area, and vice versa. The corrosion evaluation is presented in table 3.

Table 3. Corrosion area on the basis of the corresponding sorting [12]

Estimate of corrosion area, A (%)	Numerical score of corrosion damage (score points)
0.01	10
$A \leq 0.02$	9.8
$0.02 < A \leq 0.05$	9.5
$0.05 < A \leq 0.07$	9.3
$0.07 < A \leq 0.10$	9
$0.10 < A \leq 0.25$	8
$0.25 < A \leq 0.50$	7
$0.50 < A \leq 1.00$	6
$1.0 < A \leq 2.5$	5
$2.5 < A \leq 5$	4
$5 < A \leq 10$	3
$10 < A \leq 25$	2
$25 < A \leq 50$	1
$50 < A$	0

Fig. 9 shows the appearance of CP Ti samples with a coarse-grained microstructure after corrosion tests in a salt spray chamber.

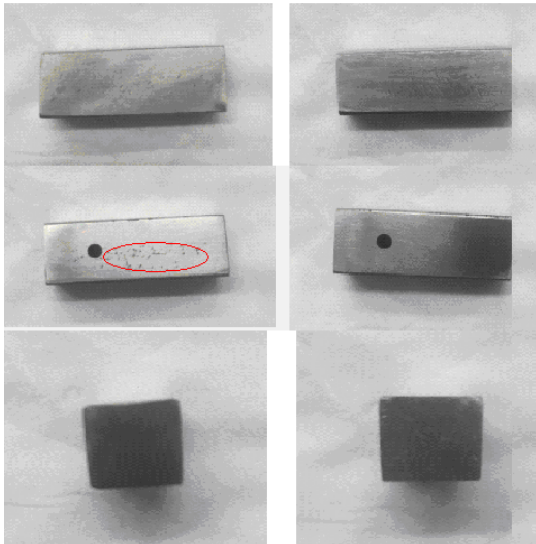


Fig. 9. Appearance of the samples with a CG structure after corrosion tests

caused by corrosion damage. The most illustrative regions of corrosion damage are marked in red on the samples with different microstructures.

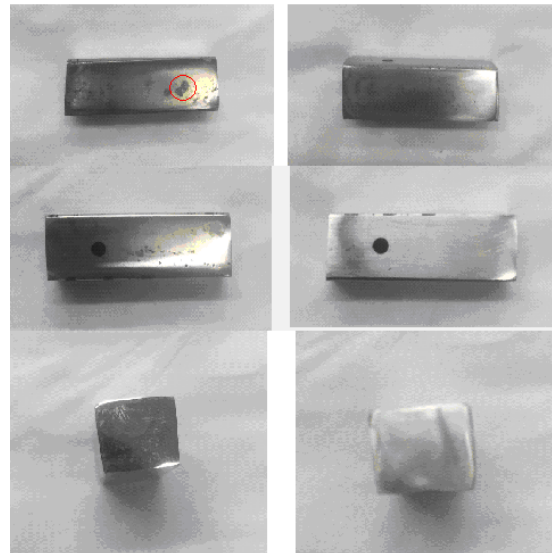


Fig. 10. Appearance of the samples with a UFG structure after corrosion tests

Fig. 10 shows the appearance of the CP Ti samples with an ultrafine-grained microstructure after corrosion tests in a salt spray chamber.

As it can be seen in Fig. 9, the corrosion damage of the samples with a CG structure is represented primarily by small, but densely spaced, point defects, as well as by rather extensive continuous areas. Apparently, such a difference is conditioned by a dissimilar surface preparation (polishing) prior to the experiment. In Fig. 10 visible are more extensive widely-spaced point defects,

However, the weighing of the samples prior to and after the corrosion tests reveals that the weight loss for the material with a CG structure is much larger than the weight loss for the samples with a UFG structure.

Table 4 presents the experimental results of corrosion tests.

Table 4. Experimental results

Sample weight, g	CG structure	UFG structure
Prior to the tests	8.274	8.524
After the tests	8.2397	8.5112
Weight loss, %	0.415	0.150
Area of corrosion damage according to Table 3	$0.07 < A \leq 0.10$	$0.05 < A \leq 0.07$
Corrosion damage score	8.2	9.3

Analysis of the table reveals that for CP Ti with a CG structure the corrosion damage under salt spray conditions is more than 2.5 times larger than the corrosion damage for the SPD-processed material with a UFG structure. This confirms the results obtained earlier.

Fig. 11 shows an electronic image of a corrosion damage region on the surface of CP Ti with a UFG structure, together with chemical analysis data.

Table 5 presents the chemical compositions corresponding to the spectra shown in fig. 11.

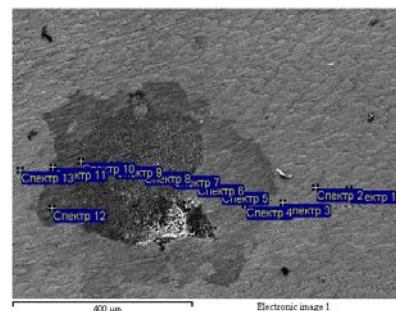


Fig. 11. Image of a corrosion damage region for the material with a UFG structure.

Table 5. Analysis of the chemical composition of the corrosion spot for CP Ti with a UFG structure.

Spectrum	O	F	Na	Si	K	Ca	Ti	Fe
Spectrum 1							100.00	
Spectrum 2							96.85	
Spectrum 3							100.00	
Spectrum 4	24.87		0.33				74.80	
Spectrum 5	25.51						74.49	
Spectrum 6	20.30	0.82	0.31				76.35	
Spectrum 7	23.00	1.18	0.79		0.28		74.75	
Spectrum 8	28.91	0.79	1.02	0.33	0.24	0.37	68.00	0.33
Spectrum 9	27.96	1.57	0.94				69.53	
Spectrum 10	25.64	0.99	0.42			0.20	68.47	0.29
Spectrum 11	26.92						70.70	

Spectrum 12	23.82		0.32				72.61	
Spectrum 13	15.85						81.01	
Max.	28.91	1.57	1.02	0.33	0.28	0.37	100.00	0.33
Min.	15.85	0.79	0.31	0.33	0.24	0.20	68.00	0.29

Proceeding from the above, the following factors can be mentioned that influence the corrosion behavior of CP Ti: grain size, the oxide film thickness, composition and continuity, electrolyte composition.

Conclusions

1. The type of the used coating (applied by ion plasma spraying or microarc oxidation) has practically no effect on the corrosion damage value of CP Ti samples.
2. The studied material (CP Ti) without coating in the ultrafine-grained state after SPD processing has a much smaller degree of corrosion damage, approximately 3 times smaller, as compared to the initial (as-annealed) state having a coarse-grained structure.
3. For the studied material with a UFG structure, a much lower corrosion rate is revealed in a 3.5% aqueous solution of sodium chloride in the observed time interval.
4. It has been established that the corrosion currents of CP Ti in the CG and UFG states in a weak-acid chloride electrolyte are different. The smaller is the grain size, the smaller is the corrosion current, which may be related to the self-passivation phenomenon and the regularities in the growth and structure of oxide films.
5. The corrosion behavior of CP Ti is influenced by grain size, oxide film composition and continuity, electrolyte composition.

ACKNOWLEDGEMENTS

The authors gratefully acknowledge the financial support under the joint Russian-Taiwanese research project RFBR No. 15-58-52015 HHC_a and MOST No. 104-2923-E-011-003-MY3.

REFERENCES:

- [1]. R.Z. Valiev, A.P. Zhilyaev, T.G. Langdon, Bulk Nanostructured Materials: Fundamentals and Applications, 2014 by John Wiley & Sons, Inc., 456 pages.
- [2]. R.Z. Valiev, Fabrication of nanostructured metals and alloys with unique properties by means of severe plastic deformation techniques. Rossiiskie Nanotekhnologii, 2006, Vol. 1, Nos. 1-2, pp. 208-216 (in Russian).

[3]. G.I. Raab, R.Z. Valiev, Equal-channel angular pressing of long-length billets. Izvestiya Vuzov. Tsvetnaya Metallurgiya, 2000, No. 5, pp.50-53 (in Russian).

[4]. Sergueeva, A.V., Stolyarov, V.V., Valiev, R.Z., Mukherjee, A.K. Advanced mechanical properties of pure titanium with ultra-fine grained structure//Scripta Materialia (2001), 45, 747-752.

[5]. N.A. Amirhanova, A.F. Razyapova, Investigation of Corrosion Properties St.3 in Coarse-Grained and Ultra Fine-Grained Conditions//Book of Abstracts on the International Symposium «Bulk Nanostructured Materials: from fundamentals to innovations» (BNM-2007), Ufa, 2007, p. 166.

[6]. G.I. Raab, V.I. Semenov, N.V. Savel'eva, E.F. Mustafina, Influence of thermo-mechanical treatment on structure and corrosion properties of carbon steels //Forging and Stamping Production. Material Working by Pressure. 2008. No. 12. pp. 34 – 36 (in Russian).

[7]. Chuan Ting Wang, Nong Gao, Mark G. Gee, et al. Processing of an ultrafine-grained titanium by high-pressure torsion: An evaluation of the wear properties with and without a TiN coating//Journal of the Mechanical Behavior of Biomedical Materials 17 (2013) pp. 166–175.

[8]. Chuan Ting Wang, Nong Gao, Mark G. Gee, et al. Tribology testing of ultrafine-grained Ti processed by high-pressure torsion with subsequent coating//J. Mater. Sci., Vol. 48, No. 13 (2013), pp. 4742-4748.

[9]. Chuan Ting Wang, Ana Escudeiro, Tomas Polcar et al. Indentation and scratch testing of DLC-Zr coatings on ultrafine-grained titanium processed by high-pressure torsion// Wear, Vol. 306, Nos. 1-2 (2013) pp. 304-310.

[10]. ASTM G31-72 (Reapproved 1999): Standard Practice for Laboratory Immersion Corrosion Testing of Metals, ASTM International.

[11]. ASTM G1-90 (Reapproved 1999): Standard Practice for Preparing, Cleaning, and Evaluating Corrosion Test Specimens, ASTM International.

[12]. Methods of Salt Spray Testing CNS8886, Bureau of Standards, Metrology & Inspection, M. O. E. A., R. O. C., 2002.